

PFC/JA-87-33

**Self-Consistent Simulation of Cyclotron**

**Autoresonance Maser Amplifiers**

K.D. Pendergast, B.G. Danly, R.J. Temkin, and J.S. Wurtele

Plasma Fusion Center

Massachusetts Institute of Technology

Cambridge, MA 02139

August 15, 1987

Revised: December 7, 1987

Submitted for publication for the IEEE Trans. on Plasma Science

Special Issue on High-Power Microwaves

## ABSTRACT

A self-consistent, one-dimensional model of the cyclotron autoresonance maser (CARM) amplifier is developed, and numerical simulations based on this model are described. Detailed studies of the CARM gain and efficiency for a wide range of initial energy and velocity spreads are presented. The interaction efficiency is found to be substantially increased when the axial magnetic field is tapered. For example, efficiencies of greater than 41% are obtained for a 140 GHz CARM amplifier with a tapered axial magnetic field and a 700 kV, 4.5 A electron beam with parallel velocity spreads of less than 1%. A discussion of the nonlinear bandwidth and interaction sensitivity to axial field inhomogeneities is presented.

## I. INTRODUCTION

The efficient generation of high-power coherent radiation in the millimeter and sub-millimeter regions of the electromagnetic spectrum has received considerable attention in the past decade. Sources capable of high power operation in these spectral regions are of interest for many applications including the electron cyclotron resonance heating of fusion plasmas and high resolution radar. Much of this interest has been focused on cyclotron resonance masers such as the gyrotron [1], gyro-klystron [2], gyro-traveling wave amplifier [3], and the doppler-shifted cyclotron resonance maser, also called the cyclotron autoresonance maser (CARM) [4–14]. Interest in the CARM results from its potential for high-efficiency operation, large doppler upshift from the cyclotron frequency, and high power capability. The cyclotron autoresonance maser is the subject of this paper.

The general cyclotron resonance condition is given by

$$\omega - \mathbf{k} \cdot \mathbf{v}_e = \frac{n\omega_{co}}{\gamma} \quad (1)$$

where  $\omega$  and  $\mathbf{k}$  are the wave frequency and wave number, and  $\mathbf{v}_e$  and  $\gamma$  are the electron velocity and the relativistic energy factor. The nonrelativistic cyclotron frequency is given by  $\omega_{co} = e|\mathbf{B}|/m$  and  $n$  is the harmonic number. For gyrotron operation, the wave is near cutoff ( $k \approx k_\perp$ , where  $k_\perp$  is the component of the wave number normal to the uniform magnetic field), and consequently the doppler shift term is small, i.e.  $\omega \sim n\omega_{co}/\gamma \gg \mathbf{k} \cdot \mathbf{v}_e$ . In the case of the CARM, the doppler shift term ( $\mathbf{k} \cdot \mathbf{v}_e$ ) is comparable to  $\omega$  and leads to a large frequency upshift. Typically, for the CARM, when  $\gamma^2 \gg 1$ ,  $\beta_\phi \approx 1$ ,  $\beta_\parallel \approx 1$ , and  $\beta_\perp \approx 1/\gamma$ , the upshift is approximately  $\gamma^2$  as seen from the resonance condition

$$\omega = \frac{n\omega_{co}}{\gamma(1 - \beta_\parallel/\beta_\phi)} \approx \frac{n\omega_{co}}{\gamma(1 - \beta_\parallel)} \approx \frac{n\omega_c}{(1 - (1 - \frac{1}{\gamma^2}))} = \gamma^2 n\omega_c \quad (2)$$

where  $\omega_c = \omega_{co}/\gamma$  is the relativistic cyclotron frequency,  $\beta_\parallel$  and  $\beta_\perp$  are the normalized axial and perpendicular electron velocities, respectively, and  $\beta_\phi = \omega/ck_\parallel$  is the normalized wave phase velocity. The choice for  $\beta_\perp$  in (2) was taken to be  $1/\gamma$ , which has been shown

to optimize the efficiency in the  $\gamma^2 \gg 1$  limit [4]. Because of this doppler upshift, the CARM requires a significantly lower magnetic field (by a factor of  $1/\gamma^2$ ) when compared with a gyrotron operating at the same frequency.

The efficiency of the CARM can also be relatively high. For an electron moving in a constant amplitude wave,  $\gamma(1 - \beta_{\parallel}\beta_{\phi})$  is a constant of the motion [15]. Therefore, in the case of luminous waves ( $\beta_{\phi} = 1$ ), an electron which is injected in resonance with the wave will remain in resonance as can be seen from (2). This effect is called cyclotron autoresonance [15]. The potential for high-efficiency operation of the CARM results from operation near exact autoresonance ( $\beta_{\phi} \gtrsim 1$ ).

Early work on CARM oscillator and amplifier theory has included the following: Soviet researchers have developed a one-dimensional theory to calculate the nonlinear efficiency of CARM oscillators and amplifiers (Bratman et al [4, 5] and Ginzburg et al. [6]). Fliflet has presented a comprehensive theory for *TE* and *TM* mode interactions [9]. Vomvoridis and Sprangle developed linear and nonlinear analyses for the CARM interaction for arbitrary phase velocity in open resonators [12]. Kreischer et al. [16] also provided a comprehensive linear theory at arbitrary angle. Finally computer simulations of the CARM amplifier have been done by Lin and coworkers [10, 11, 14]. The potential for high-efficiency operation of CARM oscillators (with a constant amplitude wave) has been demonstrated by several authors [4, 12]. Analytical studies have been done by Ride and Colson [17] for the linear theory and by Gell et al. [18] for the nonlinear theory of the CARM oscillator. Fruchtman and Friedland [19] have also analyzed a similar interaction with a nonuniform initial distribution in phase and momentum.

The efficiency of CARM amplifiers for a cold electron beam with a uniform magnetic field has been presented as a function of normalized system parameters [4, 9]. The performance of CARM amplifiers including electron beam temperature is studied here. The influence of the beam velocity and energy spreads on the gain, saturation length, and efficiency is examined with a one-dimensional nonlinear numerical simulation. Numerical results on the effects of magnetic field tapering are also presented; higher efficiencies than those calculated using optimized system parameters with a uniform magnetic field are obtained.

This paper is organized as follows: In section II, the basic theory is presented, and equations used in the simulations are derived. Section III contains the results of the numerical simulations. These include: 1) effects of input power on saturation length, 2) effects of energy and axial velocity spreads on the total efficiency, 3) effects of a linear taper of the axial magnetic field on the overall efficiency, and 4) the calculation of the nonlinear bandwidth and the effect of axial inhomogenities in the guide magnetic field. In section IV, the consequences of these results for CARM amplifier design are discussed.

## II. THEORY

### A. 1-D CARM Model

We consider an electron beam traveling along a uniform magnetic field with a co-propagating electromagnetic wave. Here it is assumed that the variation in the vector potential with the transverse coordinates can be ignored, i.e., the fields are one-dimensional. The geometry of the one-dimensional model is shown in Fig. (1). The vector potential of the signal fields for a circularly polarized wave is given by

$$\mathbf{A}_s = -A_+(z)[\sin \phi_s(z, t), -\cos \phi_s(z, t), 0] \quad (3)$$

where  $\phi_s(z, t) = \omega t - k_{\parallel} z + \delta(z)$  and  $\omega = ck$ . The slowly varying self-consistent amplitude and phase shift of the wave are, respectively,  $A_+(z)$  and  $\delta(z)$ . The slow variation of amplitude and phase requires  $1/A_+(dA_+/dz)$ ,  $(1/A_+k_{\parallel})(d^2 A_+/dz^2)$ ,  $d\phi/dz$ , and  $1/k_{\parallel}(d^2 \phi/dz^2) \ll k_{\parallel}$ . Therefore,  $\mathbf{E}_s$  and  $\mathbf{B}_s$  are given by

$$\mathbf{B}_s = \nabla \times \mathbf{A}_s = \frac{\partial}{\partial z}[-A_{s,y}\hat{x} + A_{s,x}\hat{y}] \approx -k_{\parallel} A_+[\sin \phi_s, -\cos \phi_s, 0] \quad (4)$$

$$\mathbf{E}_s = -\frac{\partial \mathbf{A}_s}{\partial t} = \omega A_+[\cos \phi_s, \sin \phi_s, 0]. \quad (5)$$

With these assumptions for the fields, a self-consistent set of equations to describe the CARM interaction can be formulated. Let  $\hat{z}$  be the direction of the uniform guide field,  $\mathbf{B}_0$ . The equations of motion are

$$\frac{d\varepsilon}{dt} = -e\mathbf{v}_e \cdot \mathbf{E}_s \quad (6)$$

$$\frac{d}{dt}(\mathbf{p}) = -e(\mathbf{E}_s + \mathbf{v}_e \times \mathbf{B}_s + \mathbf{v}_e \times \mathbf{B}_0) \quad (7)$$

$$\beta = \beta_{\parallel}[0, 0, 1] + \beta_{\perp}[\cos\Psi, \sin\Psi, 0] \quad (8)$$

where  $\varepsilon = \gamma mc^2$  and  $\mathbf{p} = \gamma\beta mc$ . The normalized parallel and perpendicular velocity as well as the particle phase are defined by (8). It is advantageous to consider  $z$  as the independent variable. Then the equations of motion can be rewritten in terms of the relativistic variables  $(\gamma, \beta_{\perp}, \beta_{\parallel})$  and a slowly varying phase  $(\theta)$ :

$$\frac{d\gamma}{dz} = -a_+ k \frac{\beta_{\perp}}{\beta_{\parallel}} \sin\theta \quad (9)$$

$$\frac{d\theta}{dz} = -\frac{a_+ k}{\gamma\beta_{\perp}\beta_{\parallel}} \left(1 - \frac{\beta_{\parallel}}{\beta_{\phi}}\right) \cos\theta + \tilde{\Delta} - \frac{d\delta}{dz} \quad (10)$$

$$\frac{d\beta_{\perp}}{dz} = \frac{a_+ k}{\gamma\beta_{\parallel}} \left(\beta_{\perp}^2 - 1 + \frac{\beta_{\parallel}}{\beta_{\phi}}\right) \sin\theta \quad (11)$$

$$\beta_{\parallel} = [1 - 1/\gamma^2 - \beta_{\perp}^2]^{1/2} \quad (12)$$

where  $a_+ \equiv eA_+/mc$ ,  $\tilde{\Delta} \equiv \omega_{co}/\gamma c\beta_{\parallel} - k(1 - \beta_{\parallel}/\beta_{\phi})/\beta_{\parallel}$ , and  $\theta \equiv \Psi - \phi_s - \pi/2$ . To close the set of equations, we use the wave equation to derive expressions for evolution of the vector potential amplitude,  $A_+(z)$ , and phase,  $\delta(z)$ :

$$-\nabla^2 \mathbf{A}_s = \mu_0 \mathbf{J} - \frac{1}{c^2} \frac{\partial^2}{\partial t^2} (\mathbf{A}_s). \quad (13)$$

Using the assumed form for the vector potential, this expression becomes

$$-2k_{\parallel} A'_+(z) \hat{\mathbf{e}}_2 + 2k_{\parallel} A_+(z) \delta'(z) \hat{\mathbf{e}}_1 = \mu_0 \mathbf{J} \quad (14)$$

where we have defined unit vectors  $\hat{\mathbf{e}}_1 \equiv [\sin \theta_s, -\cos \theta_s, 0]$  and  $\hat{\mathbf{e}}_2 \equiv [\cos \theta_s, \sin \theta_s, 0]$ . Taking the dot product of (14) with  $\hat{\mathbf{e}}_2$ ,

$$-2k_{\parallel} A'_+(z) = \mu_0 \mathbf{J} \cdot \hat{\mathbf{e}}_2 = \mu_0 \mathbf{J}_{\perp} \cdot \hat{\mathbf{e}}_2. \quad (15)$$

Since  $k_{\parallel}$  and  $A_+(z)$  are assumed independent of time and the transverse coordinates, the right-hand side of (15) is then averaged over time and the beam cross section while summing over all the electrons. Solving (15) for  $a'_+(z)$ , we obtain

$$a'_+(z) = \frac{\mu_0 e}{mc} \frac{J_{0eff}}{2k_{\parallel}} \left\langle \frac{\beta_{\perp}(z)}{\beta_{\parallel}(z)} \sin \theta(z) \right\rangle \quad (16)$$

Similarly, taking the dot product of (14) with  $\hat{\mathbf{e}}_1$ , one obtains an expression for the self-consistent change in the wave phase due to interaction with the beam:

$$\delta'(z) = \frac{\mu_0 e}{mc} \frac{J_{0eff}}{2k_{\parallel} a_+} \left\langle \frac{\beta_{\perp}(z)}{\beta_{\parallel}(z)} \cos \theta(z) \right\rangle \quad (17)$$

where  $J_{0eff}$  is the effective current density (see (21)). Equations (9 – 12, 16, 17) constitute a complete, one-dimensional self-consistent description of a CARM amplifier including TE waveguide modes.

### B. Waveguide Modes

We have assumed, in this one-dimensional model, that the wave amplitude is uniform over the entire cross section of the electron beam. To treat waveguide modes in this context, the field seen by the particles must be related to the total power in the waveguide. We consider  $TE_{mn}$  waveguide modes. In a circular waveguide, the boundary condition yields a relation between the pipe radius,  $a$ , and  $\nu_{mn}$ , the  $n^{\text{th}}$  zero of the Bessel function  $J'_m(x)$ :

$$a = \frac{\nu_{mn}}{k_{\perp}} = \frac{\nu_{mn}}{k(1 - \beta_{\phi}^{-2})^{1/2}}. \quad (18)$$

If  $P/dS$  is the power per unit area on axis at the position of the electron beam and  $P_{tot}$  is the total power flow in the guide, then for  $TE_{mn}$  modes, the ratio of the two is [20]

$$\frac{P/dS}{P_{tot}} = \frac{1}{\pi a^2} \left\{ \frac{\nu_{mn}^2}{(\nu_{mn}^2 - m^2) J_m^2(\nu_{mn})} \right\}. \quad (19)$$

The power density,  $P/dS$ , can then be related to the normalized vector potential  $a_+(z)$ . For the case of  $TE_{mn}$  waveguide modes, the effective current density in (16) can be expressed as

$$J_{0eff} = \frac{I_0 k^2 \beta_\phi}{2\pi(\nu_{mn}^2 - m^2) J_m^2(\nu_{mn})}. \quad (20)$$

The two-dimensional effects of waveguide modes can be accurately handled in this one-dimensional model provided that the variation of the fields are insignificant. This one-dimensional model neglects the variation of the field across the electron beam; a two-dimensional model which takes this variation into account is presently under development and will be discussed in a future paper.

### C. Growth Rate

Although a single particle in autoresonance with a wave can transfer most of its energy to the wave, given a sufficient interaction length and proper initial phase, the electrons in a real beam are initially uniformly distributed in phase. As a result, the optimum interaction efficiency occurs not at exact autoresonance, but rather for a wave phase velocity which is slightly greater than the speed of light [4]. In practice, for high frequency devices operating with waveguide electromagnetic modes and with uniform axial fields, usual system parameters are such that the efficiency is increased by decreasing the wave phase velocity. On the other hand, the CARM growth rate increases quickly with increasing wave phase velocity (see below, [4, 9]). Therefore, in this paper, we will restrict discussion to the case of non-luminous waves ( $\beta_\phi \neq 1$ ). In the design of practical devices, the optimal choice of  $\beta_\phi$  is determined by consideration of the tradeoff between the desired efficiency and an adequate growth rate. The growth rate must be both sufficiently high to overcome velocity and energy spreads present in the beam and to limit the device length to a reasonable value.



Let the dimensionless vector potential scale as  $a_+ \sim \exp[i(\Gamma - \Delta)\varsigma]$  where  $\Delta$  and  $\varsigma$  are the normalized detuning and length defined by

$$\Delta \equiv \frac{2(1 - \beta_{\parallel 0}/\beta_\phi)}{\beta_{\perp 0}^2(1 - \beta_\phi^{-2})} \left(1 - \frac{\beta_{\parallel 0}}{\beta_\phi} - \frac{\omega_c}{\omega}\right), \quad (21)$$

$$\omega_{b0} \equiv \left(\frac{e^2 n}{\epsilon_0 m}\right)^{1/2}, \quad (22)$$

$$\varsigma = \frac{\beta_{\perp 0}^2(1 - \beta_\phi^{-2})}{2(1 - \beta_{\parallel 0}/\beta_\phi)} \frac{\omega z}{c\beta_{\parallel 0}}. \quad (23)$$

When the dimensionless parameter  $I$ , defined by

$$I \equiv \frac{4\beta_{\parallel 0}(1 - \beta_{\parallel 0}/\beta_\phi)^3}{\beta_{\perp 0}^4(1 - \beta_\phi^{-2})^2} \frac{\omega_{b0}^2}{\omega^2} \quad (24)$$

satisfies  $I \ll 1$ , a small-signal analysis of the CARM amplifier results in a dispersion relation similar to the well-known TWT dispersion relation [4]:

$$(\Gamma - \Delta)\Gamma^2 = \frac{I}{2}. \quad (25)$$

The normalized field growth rate is maximized for  $\Delta = 0$  and is given by

$$Im \Gamma = \frac{\sqrt{3}}{2} \left[\frac{I}{2}\right]^{\frac{1}{3}}. \quad (26)$$

This corresponds to a spatial field growth rate of

$$Im \Gamma_k = 0.0493 \left[ \frac{J_{0eff} k \theta_{p0}^2 (1 - \beta_\phi^{-2})}{\gamma_0 \beta_{\parallel 0}} \right]^{1/3} [m^{-1}] \quad (27)$$

where  $J_{0eff}$  is the effective current density in A/m<sup>2</sup> and is given in (20),  $k$  is the magnitude of the wave number in m<sup>-1</sup>, and the initial pitch angle,  $\theta_{p0}$ , is given by  $\theta_{p0} = \beta_{\perp 0}/\beta_{\parallel 0}$ .

### III. SIMULATIONS

#### A. Numerical Model

In order to investigate the effect of both velocity and energy spreads in the electron beam and magnetic field tapering on CARM amplifiers, a numerical simulation of the one-dimensional model presented in the previous section was developed. In this section, we describe the implementation of this model and discuss its results.

In this particle simulation of the CARM interaction, the averages on  $a_+$  and  $\delta$  must be defined. We define the averages in (16, 17) by

$$\langle ( \quad ) \rangle \equiv \frac{1}{N_p} \sum_{i=1}^{N_p} ( \quad )_i. \quad (28)$$

The complete system of self-consistent CARM amplifier equations is then

$$\frac{d\gamma_i}{dz} = -a_+ k \frac{\beta_{\perp i}}{\beta_{\parallel i}} \sin \theta_i \quad (29)$$

$$\frac{d\theta_i}{dz} = \frac{\omega_{co}}{\gamma_i c \beta_{\parallel i}} - \frac{k}{\beta_{\parallel i}} \left(1 - \frac{\beta_{\parallel i}}{\beta_{\phi}}\right) - \frac{a_+ k}{\gamma_i \beta_{\perp i} \beta_{\parallel i}} \left(1 - \frac{\beta_{\parallel i}}{\beta_{\phi}}\right) \cos \theta_i - \frac{d\delta}{dz} \quad (30)$$

$$\frac{d\beta_{\perp i}}{dz} = \frac{a_+ k}{\gamma_i \beta_{\parallel i}} (\beta_{\perp i}^2 - 1 + \frac{\beta_{\parallel i}}{\beta_{\phi}}) \sin \theta_i \quad (31)$$

$$\beta_{\parallel i} = [1 - 1/\gamma_i^2 - \beta_{\perp i}^2]^{1/2} \quad (32)$$

$$\frac{da_+}{dz} = \frac{\mu_0 e}{mc} \frac{J_{0eff}}{2k_{\parallel}} \frac{1}{N_p} \sum_{i=1}^{N_p} \frac{\beta_{\perp i}}{\beta_{\parallel i}} \sin \theta_i \quad (33)$$

$$\frac{d\delta}{dz} = \frac{\mu_0 e}{mc} \frac{J_{0eff}}{2k_{\parallel} a_+} \frac{1}{N_p} \sum_{i=1}^{N_p} \frac{\beta_{\perp i}}{\beta_{\parallel i}} \cos \theta_i. \quad (34)$$

These equations represent a system of  $3N_p + 2$  simultaneous ordinary differential equations modeling the CARM amplifier, where  $N_p$  is the total number of macroparticles in the model (typically,  $N_p = 1024$  or  $2048$ ).

In the simulations, the particles are loaded, using Hammersley's bit-reversed algorithm [21], with Gaussian distributions in  $\gamma$  and  $\beta_{\parallel}$  and a uniform distribution in  $\theta$ . These Gaussian distributions of initial  $\gamma$  and  $\beta_{\parallel}$  values are characterized by standard deviations of  $\sigma_{\gamma}$  and  $\sigma_{\beta_{\parallel}}$ , respectively. We define the spreads in the beam energy,  $\gamma$ , and axial velocity,  $\beta_{\parallel}$ , in terms of the standard deviation of the respective Gaussian distributions. For example, the energy distribution,  $f(\gamma)$ , is given by:

$$f(\gamma) = \frac{1}{\sqrt{\pi}\sigma_{\gamma}} e^{-\left(\frac{\gamma-\gamma_0}{\sigma_{\gamma}}\right)^2}. \quad (35)$$

In these simulations, the distribution functions were truncated at five standard deviations. The initial value problem represented by the differential equations (30–35) is solved by a fourth order Runge-Kutta algorithm.

As the illustrative example for the following discussion, the following parameters were used in the simulation:  $\gamma = 2.37$  ( $V = 700kV$ ),  $I_0 = 4.4$  A,  $\beta_{\phi} = 1.066$ ,  $\nu = 140$  GHz,  $B \sim 2.93T$ , and  $\theta_{p0} = 0.53$ . These values are representative of one of a number of designs under development at M.I.T. The conclusions drawn from the results presented below are believed to be generally applicable to CARM amplifiers operating with other design parameters.

For the parameters listed above, simulations were carried out for a wide variety of other system parameters. A typical simulation result for the wave power as a function of interaction length is shown in Fig. (2). In this figure, the exponential high-gain regime is characterized by the straight line. The slope of this line is the growth rate and can be obtained from the roots of the cubic dispersion relation (25). For zero detuning ( $\Delta = 0$ ), the exponential growth rate is maximum, and the launching loss is  $1/9$ . In Fig. (2), the detuning corresponds to the value required for optimum efficiency ( $\Delta = 0.4$ ), and the launching loss is not the same as for the  $\Delta = 0$  case. Saturation occurs at approximately  $z = 0.3$  m, and the synchrotron oscillations of the particles in the potential well are seen for  $z > 0.3$  m.

For constant initial electron beam power, the saturated power of the wave should not vary noticeably with input power [9], although the saturation length of the interaction

should depend on the input power. For operation strictly in the exponential, high-gain regime, an increase in the input power by a factor of  $e$  should cause a decrease in the saturation length by  $1/\Gamma$ . The simulations verify that the saturated power is nearly constant over a wide range of input powers, and that the saturation length decreases with increasing input power, as predicted.

### *B. The Effect of Energy and Axial Velocity Spreads*

Of critical importance to the operation of the CARM amplifier are electron beam quality effects. With zero energy and velocity spreads in the beam, initial values of  $\gamma$  and  $\beta_{\parallel}$  can be chosen, for a given wavelength and magnetic field strength, such that all the particles have the optimum detuning from resonance. Then for  $\beta_{\phi} \approx 1$ , a large fraction of energy ( $\sim 40\%$ , see below) can be transferred from the electron beam to the wave. However, with spreads in the initial energy and axial velocity distribution of the particles, the detuning from resonance varies from particle to particle. This decreases the total efficiency, defined by

$$\eta(z) \equiv \frac{\langle \gamma_0 \rangle - \langle \gamma(z) \rangle}{\langle \gamma_0 \rangle - 1}. \quad (36)$$

In particular, the extent to which the energy and velocity spreads can be tolerated by the interaction is a crucial issue in the design of a CARM amplifier.

Spreads in the initial energy and axial velocity distributions of the electron beam were introduced into the CARM amplifier model described in the previous section. The effects of these spreads for the parameters given in Section III.A on the interaction efficiency are shown in Fig. (3) and Fig. (4). With energy and axial velocity spreads in the electron beam, the optimum detuning value is nearly equal to that of a cold beam ( $\Delta = 0.4$ , [4]), and thus the detuning value for the data presented in these figures was taken to be  $\Delta = 0.4$ .

In Fig. (3), the effect of energy spread on interaction efficiency is shown, where the axial velocity spread is negligible ( $\sigma_{\beta_{\parallel}} = 2 \times 10^{-4}$ ). Although the efficiency decreases with increasing energy spread as expected, the fall-off is modest for moderate energy spreads. Energy spread is thus unlikely to severely limit the efficiency in practical devices.

In Fig. (4), the effect of axial velocity spread on interaction efficiency is shown, where the energy spread is taken to be negligible ( $\sigma_\gamma = 2 \times 10^{-4}$ ). With axial velocity spreads  $\sigma_{\beta\parallel} < 0.005$ , high efficiencies ( $\eta \gtrsim 23\%$ ) appear feasible. However, for axial velocity spreads  $\sigma_{\beta\parallel} > 0.005$ , the total efficiency drops off dramatically with increasing velocity spread. Such a serious degradation of efficiency by modest velocity spreads is a potentially serious problem for the CARM. However, as will be shown in the following section, the rapid reduction in efficiency with increasing velocity spread can be compensated for to some extent, by tapering of the guide magnetic field.

### *C. Efficiency Enhancement Through Magnetic Field Tapering*

In order to increase efficiencies over those obtained in the previous section, magnetic field tapering is attractive. In tapering of the magnetic field, linear tapers were analyzed. The guide magnetic field was assumed to be of the form

$$\mathbf{B}(z) = \begin{cases} B_0 \hat{\mathbf{z}}, & z < z_0; \\ -\frac{1}{2} B_0 \alpha r \hat{\mathbf{r}} + B_0 (1 + \alpha(z - z_0)) \hat{\mathbf{z}}, & z > z_0 \end{cases} \quad (37)$$

which is everywhere divergenceless and irrotational. It is assumed that  $\alpha$  is small so that  $|\alpha r| \ll 1$ . The contribution of the radial component of the magnetic field to the azimuthal component of the Lorentz force vanishes on axis for the one-dimensional model. However, averaging over a gyro-period yields a net axial force where  $r$  is evaluated at the Larmor radius of the electron. equation of motion for the perpendicular and parallel velocities will have an added term due to the taper. In other words,  $\beta_\perp^2/B$  becomes an adiabatic invariant (in the absence of an electromagnetic wave).

In Fig. (5), the amount to which the amplifier efficiency can be increased by magnetic tapering is shown as a function of velocity spread for a fixed linear taper ( $\alpha = -0.5\%/cm$ ). As can be seen by comparing Fig. (4) with Fig. (5), tapering the magnetic field increases the efficiency of the CARM amplifier substantially over a wide range of axial velocity spreads. In particular, the fractional increase in efficiency is even more pronounced for modest velocity spreads than for zero velocity spread. In Fig. (5), the efficiencies for both

the tapered and untapered cases at zero detuning are shown. This value of detuning gives larger tapered efficiencies than at the untapered optimum efficiency detuning  $\Delta = 0.4$ . The efficiencies for untapered magnetic field in Fig. (5) are also calculated at zero detuning, and they are therefore less than the corresponding values in Fig. (4).

In Fig. (6), the power as a function of interaction length is shown for both tapered (dashed line) and untapered (solid line) magnetic fields. In this figure, the energy spread is  $\sigma_\gamma = 0.03$  and the axial velocity spread is  $\sigma_{\beta\parallel} = 0.01$ . As can be seen, there is a substantial increase in efficiency due to the magnetic field tapering.

In Fig. (7), the longitudinal phase space of the particles is shown, for a magnetic field taper similar to that of Fig (6). The particles which are trapped and decelerated by the wave are clearly seen. The untrapped particles are not resonant with the wave and do not transfer an appreciable amount of their energy to the wave. Moreover, some are actually accelerated.

The effect of an inhomogeneity in the axial guide field on the CARM interaction was also considered. An axial magnetic field of the form

$$B(z) = B_0 \left(1 + \frac{\delta B}{B_0} \sin \hat{k}z\right) \quad (38)$$

was assumed where  $\delta B/B_0$  and  $\hat{k}$  are the amplitude and wavenumber of the spatial inhomogeneity in the axial direction. In the small-signal regime, the interaction was sensitive to the axial field homogeneity. A field fluctuation  $\delta B/B_0 < 0.1\%$ , for wavelengths  $2\pi/\hat{k}$  ranging from one-half to two times the interaction length, is required for negligible reduction of the interaction efficiency. In the nonlinear regime, where the particles are trapped, the interaction was considerably less sensitive to field homogeneity. A field inhomogeneity of  $\delta B/B_0 \sim 1\%$  results in negligible change in the tapered efficiency.

#### *D. Nonlinear Bandwidth*

The nonlinear frequency bandwidth of the CARM amplifier was investigated for the case of a non-ideal (warm) beam. An energy spread of  $\sigma_\gamma = 0.03$  and an axial velocity spread of  $\sigma_{\beta\parallel} = 0.01$  were assumed. The amplifier length was set at the saturation length

(30 cm) and the axial guide field was fixed for the design frequency  $\nu = 140$  GHz and for the optimum detuning  $\Delta = 0.4$ . The saturated gain was then calculated as a function of frequency for an input power of 100 W. For the system parameters chosen, the 3 dB nonlinear bandwidth corresponded to frequencies in the range  $\nu \in [129, 142.5]$ , or  $\Delta\nu/\nu \approx 9.6\%$ . There is a slow decrease in gain for frequencies  $\nu \leq 129$  GHz and a sharp decrease in gain at frequencies  $\nu \geq 144$  GHz; at  $\nu = 145$  GHz, the gain is 8 dB down from the value at  $\nu = 140$  GHz.

#### IV. DISCUSSION AND CONCLUSIONS

In this paper, a nonlinear, self-consistent theory of the cyclotron autoresonance maser amplifier has been presented. The results of detailed simulations of a 140 GHz CARM amplifier, including the effect of energy and velocity spreads, have been discussed. Efficiency enhancement by tapering of the axial magnetic field has been investigated as a function of axial velocity spread in the CARM amplifier has been calculated, and the interaction sensitivity to spatial fluctuations in the axial guide field has been studied.

The present results have been obtained with a one-dimensional numerical model. Although a two-dimensional treatment, such as that developed by Lin [10, 11], will necessarily provide a more detailed model of the interaction, the nonlinear model presented here and the associated numerical code can provide, with a minimum of computational effort, valuable insight into the effect of beam temperature and guide field tapering.

The potential for excitation of an absolute, rather than convective, instability in either the operating mode or other lower-order modes may exist in the CARM amplifier. This instability becomes important at sufficiently high current levels or at magnetic fields significantly larger than the grazing field [3, 7]. In the design of CARM amplifiers, the possibility of exciting this absolute instability must be considered, and design parameters must be chosen such that this instability is not excited. The present system parameters chosen as the example are believed to be stable with respect to an absolute instability, based on a detailed pinch-point analysis which has been carried out [22] and will be reported elsewhere.

In this paper, it has been shown that the detrimental effect of energy and velocity spread on efficiency in the CARM amplifier can be partially compensated for by the application of a tapered magnetic field. With a parallel velocity spread of  $\sigma_{\beta\parallel} = 0.01$ , the efficiency is increased, by tapering, from 9% to 41%. Such velocity spreads appear possible using a Pierce gun-wiggler configuration. With a cold beam, the efficiency is increased from 36% to 46% by tapering of the magnetic field.

In conclusion, the CARM interaction appears attractive for the generation of high-power, coherent radiation in the millimeter wave region of the spectrum. The sensitivity of the CARM amplifier to axial velocity spread necessitates the production of high quality electron beams.

#### ACKNOWLEDGEMENTS

This work is supported in part by the Innovative Science and Technology Office of the Strategic Defense Initiative Organization and managed by the Harry Diamond Laboratories.



## References

- [1] K.E. Kreischer and R.J. Temkin, "Single-mode operation of a high-power, step-tunable gyrotron," *Phys. Rev. Letters*, Vol. 59, pp. 547-550 (1987).
- [2] K.R. Chu, V.L. Granatstein, P.E. Latham, W. Lawson, and C.D. Striffler, "A 30-MW Gyroklystron-Amplifier Design for High-Energy Linear Accelerators," *IEEE Trans. Plas. Sci.*, Vol. PS - 13, pp. 424-434 (1985).
- [3] Y.Y. Lau, K.R. Chu, L.R. Barnett, and V.L. Granatstein, "Gyrotron Travelling Wave Amplifier," *Int. J. Infr. and Mill. Waves*, Vol. 2, pp. 373-425 (1981).
- [4] V.L. Bratman, N.S. Ginzburg, G.S. Nusinovich, M. I. Petelin, and P. S. Strelkov, "Relativistic Gyrotrons and Cyclotron Autoresonance Masers," *Int. J. Electron.*, Vol. 51, pp. 541-567 (1981).
- [5] V.L. Bratman, G.G. Denisov, N.S. Ginzburg, and M. I. Petelin, "FEL's with Bragg Reflection Resonators: Cyclotron Autoresonance Masers Versus Ubitrons," *IEEE J. Quant. Elec.*, Vol. QE - 19, pp. 282-296 (1983).
- [6] N.S. Ginzburg, I.G. Zarnitsyna, and G.S. Nusinovich, "Theory of Relativistic Cyclotron-Resonance Maser Amplifiers," *Radio Physics and Quant. Elec.*, Vol. 24, pp. 331-338 (1981).
- [7] A.T. Lin and K.R. Chu, "Stability and Tunability of a CARM Amplifier," UCLA Report PPG-1054 (1987).
- [8] P. Sprangle, Cha-Mei Tang, and P. Serafum, "Induced Resonance Electron Cyclotron (IREC) Quasi-Optical Maser," NRL Memorandum Report 5678 (1985).
- [9] A.W. Fliflet, "Linear and Nonlinear Theory of the Doppler-Shifted Cyclotron Resonance Maser Based on TE and TM Waveguide modes," *Int. J. Electron.*, Vol. 61, pp. 1049-1080 (1986).
- [10] A.T. Lin and C.C. Lin, "Doppler Shift Dominated Cyclotron Maser Amplifiers," *Int. J. Infr. and Mill. Waves*, Vol. 6, pp. 41-51 (1985).
- [11] A.T. Lin, "Doppler Shift Dominated Cyclotron Masers," *Int. J. Electron.*, Vol. 57, pp. 1097-1108 (1984).
- [12] J.L. Vomvoridis and P. Sprangle, "Linear and Nonlinear Electron Cyclotron Interaction in Open Resonators," *Phys. Rev. A*, Vol. 25, pp. 931-946.

- [13] J.L. Vomvoridis, "An Efficient Doppler-Shifted Electron-Cyclotron Maser Oscillator," *Int. J. Elect.*, Vol. 53, pp. 555-571 (1982).
- [14] A.T. Lin, W.W. Chang, and C.C. Lin, "Thermal Effects on the Efficiency of Doppler-shift Dominated Cyclotron Masers," *Phys. Fluids*, Vol. 27, pp. 1054-1057 (1984).
- [15] A.A. Kolomenskij and A.N. Lebedev, DAN SSR, 145, p. 1259 (1962).
- [16] K.E. Kreischer and R.J. Temkin, "High-Frequency Gyrotrons and their Application to Tokamak Plasma Heating," *Infrared and Mill. Waves*, Vol. 7, pp. 377-485 (1983).
- [17] S.K. Ride and W.B. Colson, "A Free-Electron Laser in a Uniform Magnetic Field," *Appl. Phys.*, Vol 20, pp. 41-50 (1979).
- [18] Y. Gell, J.R. Torstensson, H. Wilhelmsson, and B. Levush, "On a Free-Electron Laser in a Uniform Magnetic Field. A Solution for Arbitrarily Strong Electromagnetic Radiation Fields," *Appl. Phys.*, Vol B 27, pp. 15-18 (1982).
- [19] A. Fruchtman and L. Friedland, "Theory of a Nonwiggler Collective Free-Electron Laser in a Uniform Magnetic Field," *IEEE J. Quant. Electron.*, Vol QE - 19, pp. 327-333 (1983).
- [20] R.E. Collin, *Foundations for Microwave Engineering*, McGraw-Hill, New York, 1966.
- [21] J.M. Hammersley and D.C. Handscomb, *Monte Carlo Methods*, Methuen, London, 1964.
- [22] B.G. Danly, K.D. Pendergast, R.J. Temkin, and J. Davies, "Design of a High-Power, 140 GHz CARM Amplifier", submitted for publication in SPIE Proceedings, vol. 873, 1988.

### List of Figures

**Fig 1.** Schematic diagram of the CARM interaction. An electromagnetic wave is copropagating with an electron traveling along a uniform magnetic field. The component of the wavevector along the direction of the guide magnetic field is  $k_{\parallel}$ .

**Fig 2.** Power vs. distance in a CARM amplifier extending into the nonlinear regime for a cold electron beam ( $\Delta = 0.4$ ).

**Fig 3.** Effect of energy spread on the efficiency of the CARM Amplifier ( $\Delta = 0.4$ ,  $\sigma_{\beta\parallel} = 2 \times 10^{-4}$ ).

**Fig 4.** Effect of velocity spread on the efficiency of the CARM Amplifier ( $\Delta = 0.4$ ,  $\sigma_{\gamma} = 2 \times 10^{-4}$ ).

**Fig 5.** Effect of velocity spread on CARM efficiency for both tapered and untapered magnetic fields ( $\Delta = 0$ ,  $\sigma_{\gamma} = 2 \times 10^{-4}$ ).

**Fig 6.** Power vs. distance in a CARM amplifier using for an untapered (solid line) and tapered (dashed line) magnetic field ( $\Delta = 0$ ,  $\sigma_{\beta\parallel} = 0.01$ ,  $\sigma_{\gamma} = 0.03$ ,  $z_0 = 22$  cm).

**Fig 7.** Phase space of the CARM interaction with a tapered magnetic field ( $\Delta = 0$ ,  $\sigma_{\gamma} = 0.01$ ,  $\sigma_{\beta\parallel} = 0.005$ ,  $z_0 = 17$  cm).

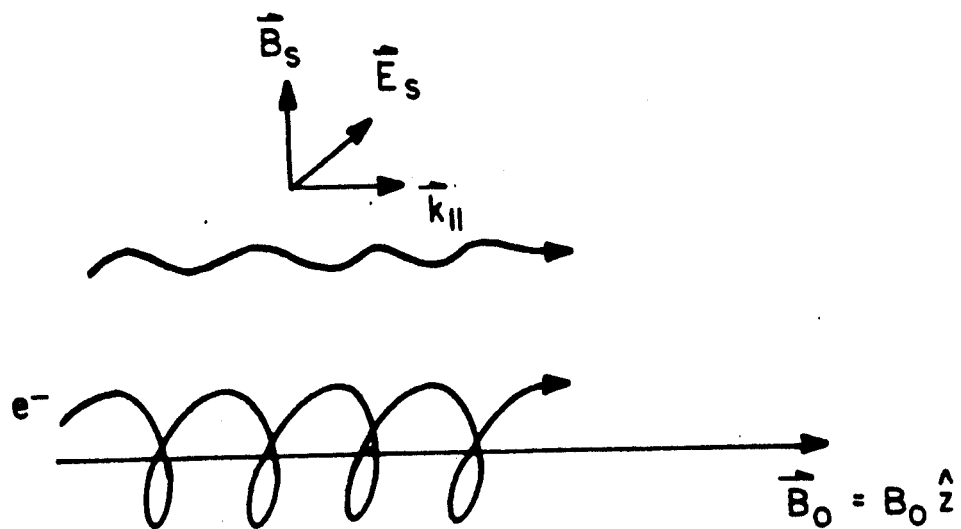


Fig 1.

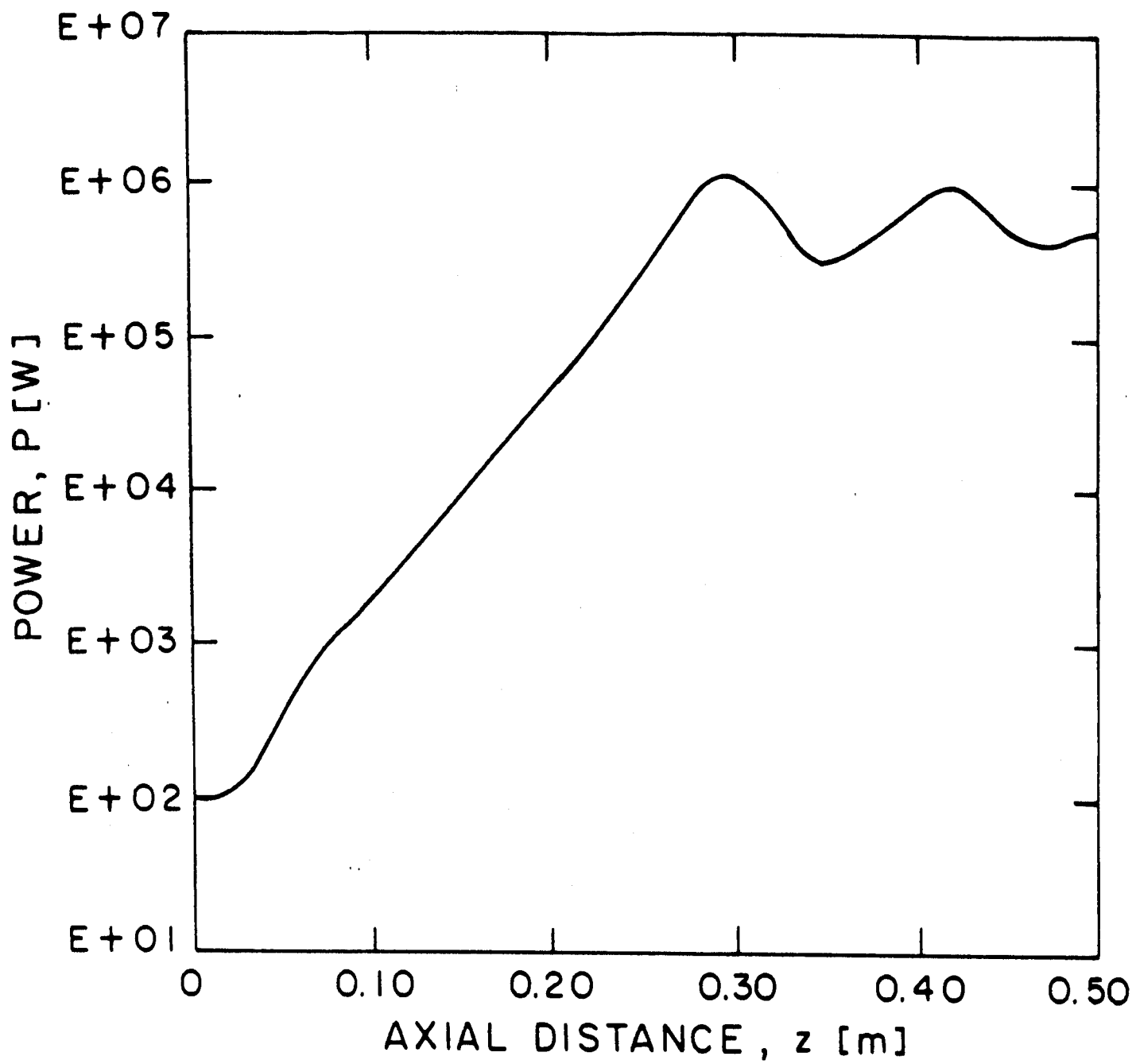


Fig 2.

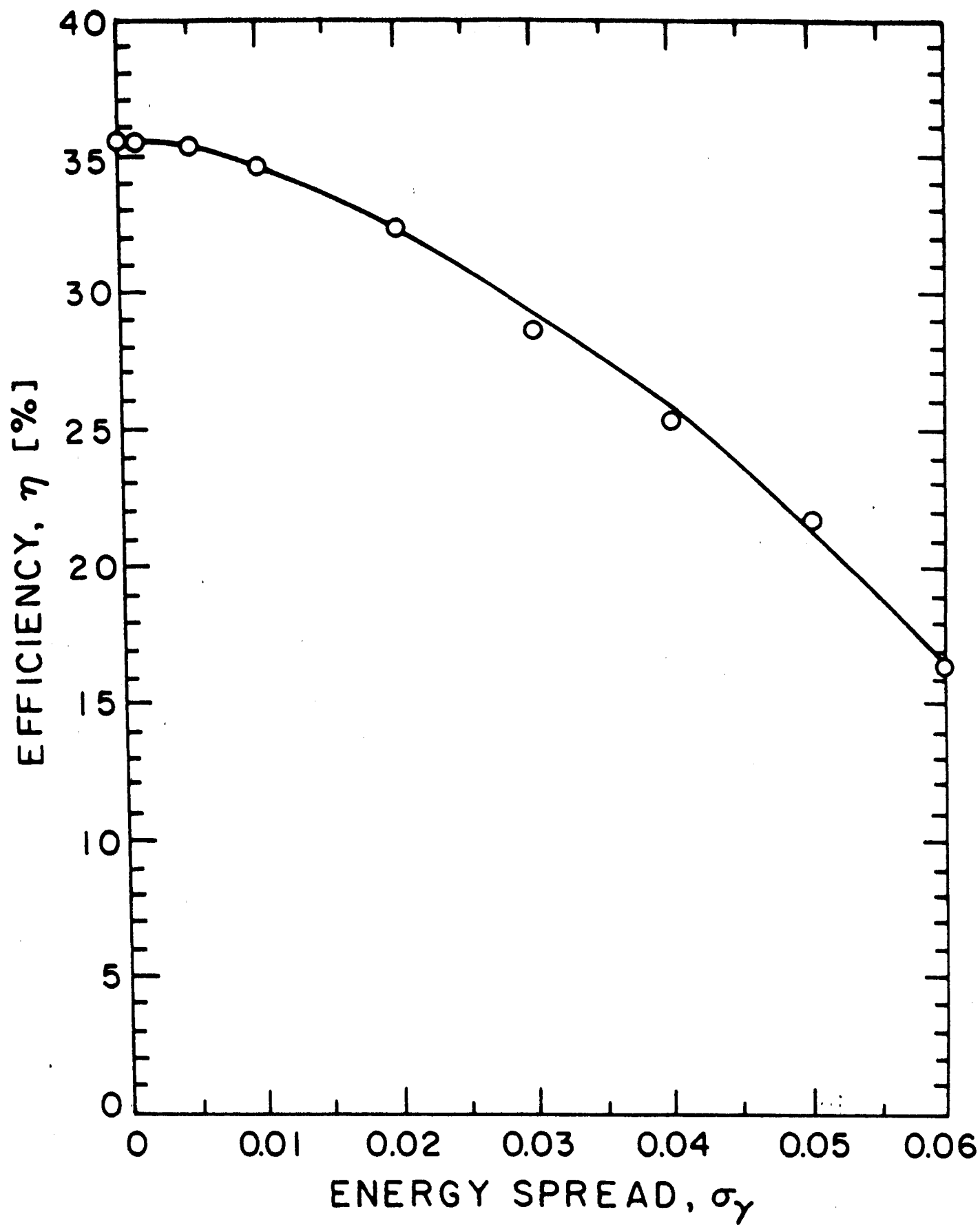


Fig 3.

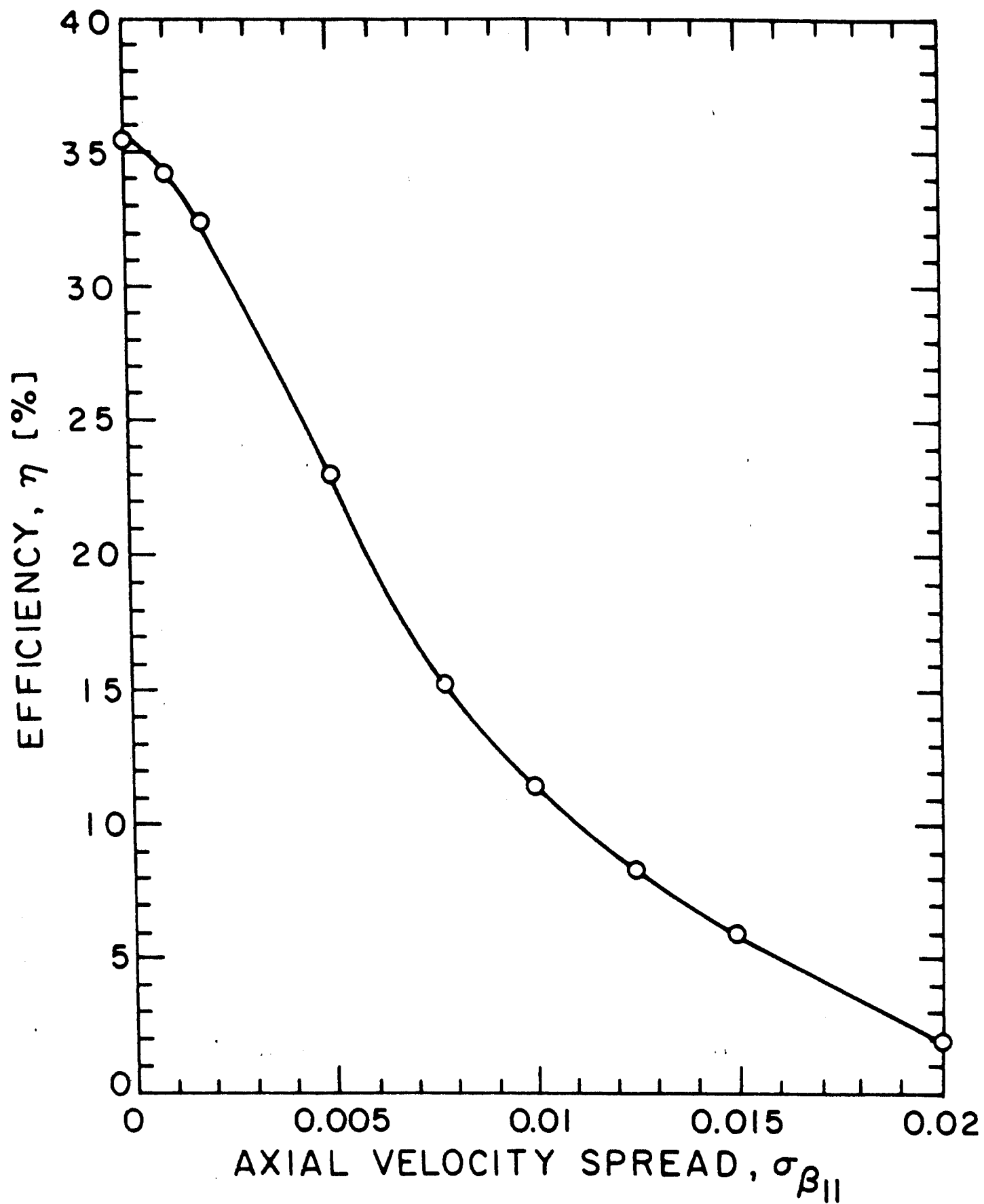


Fig 4.

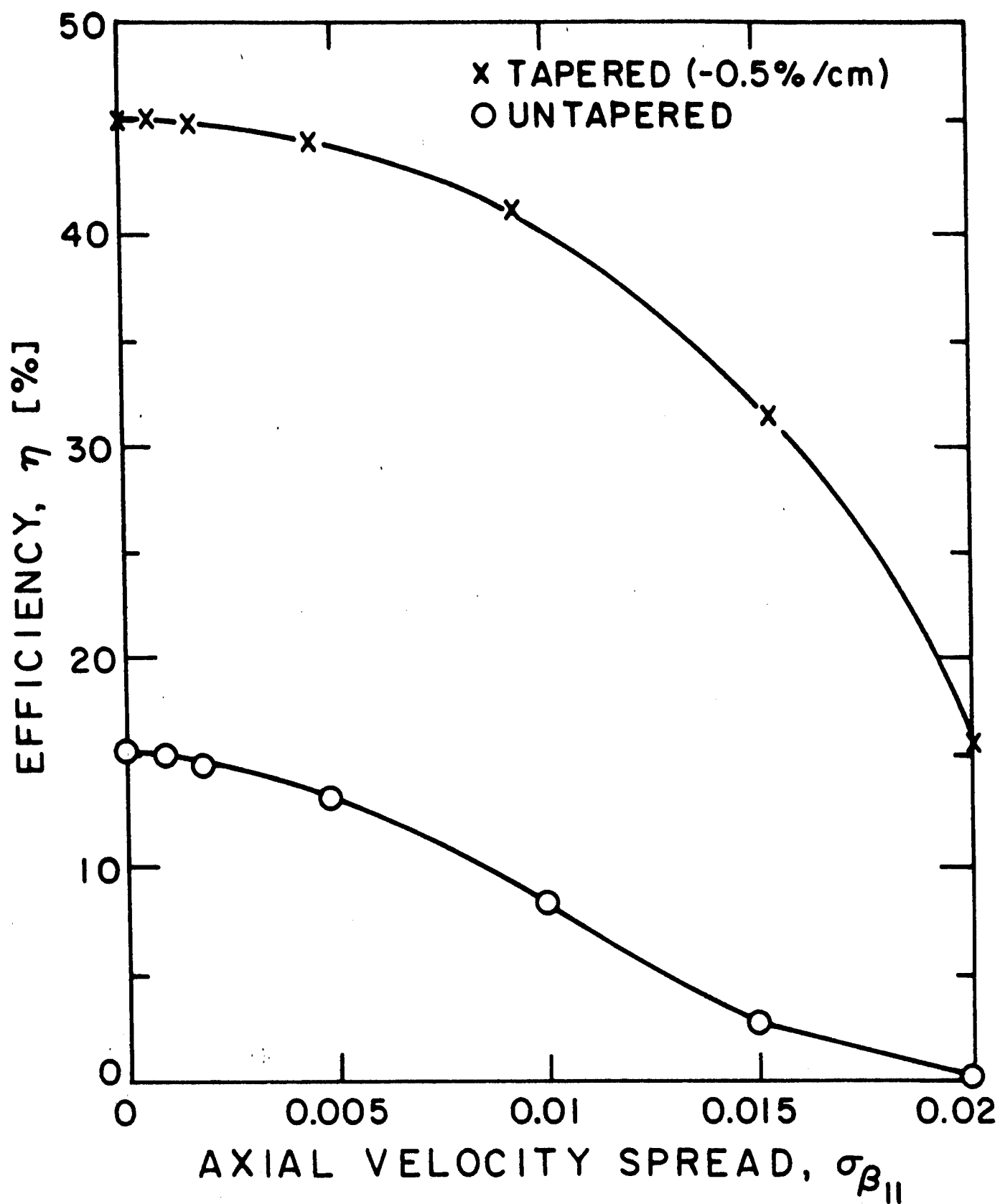


Fig 5.



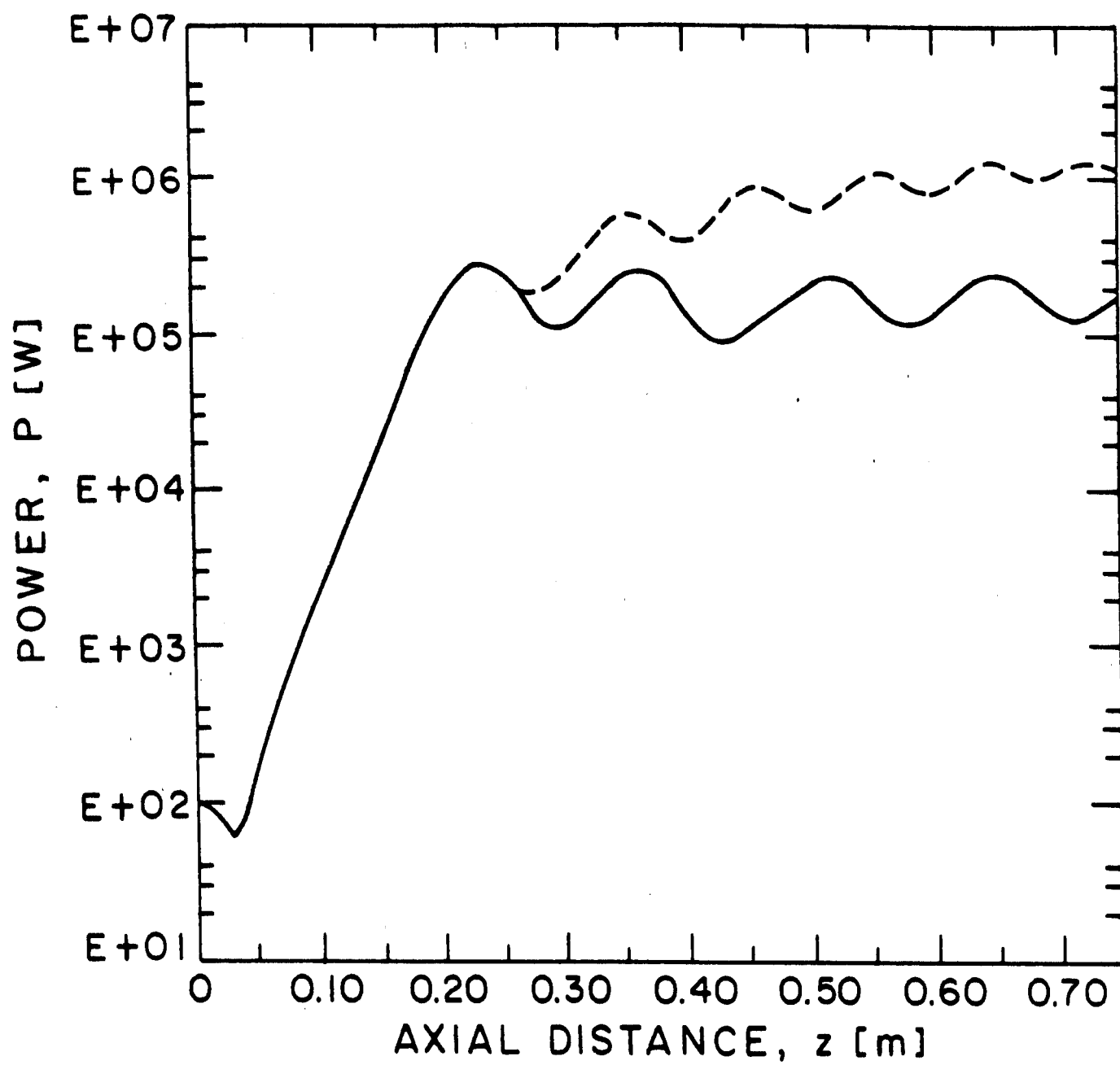


Fig 6.

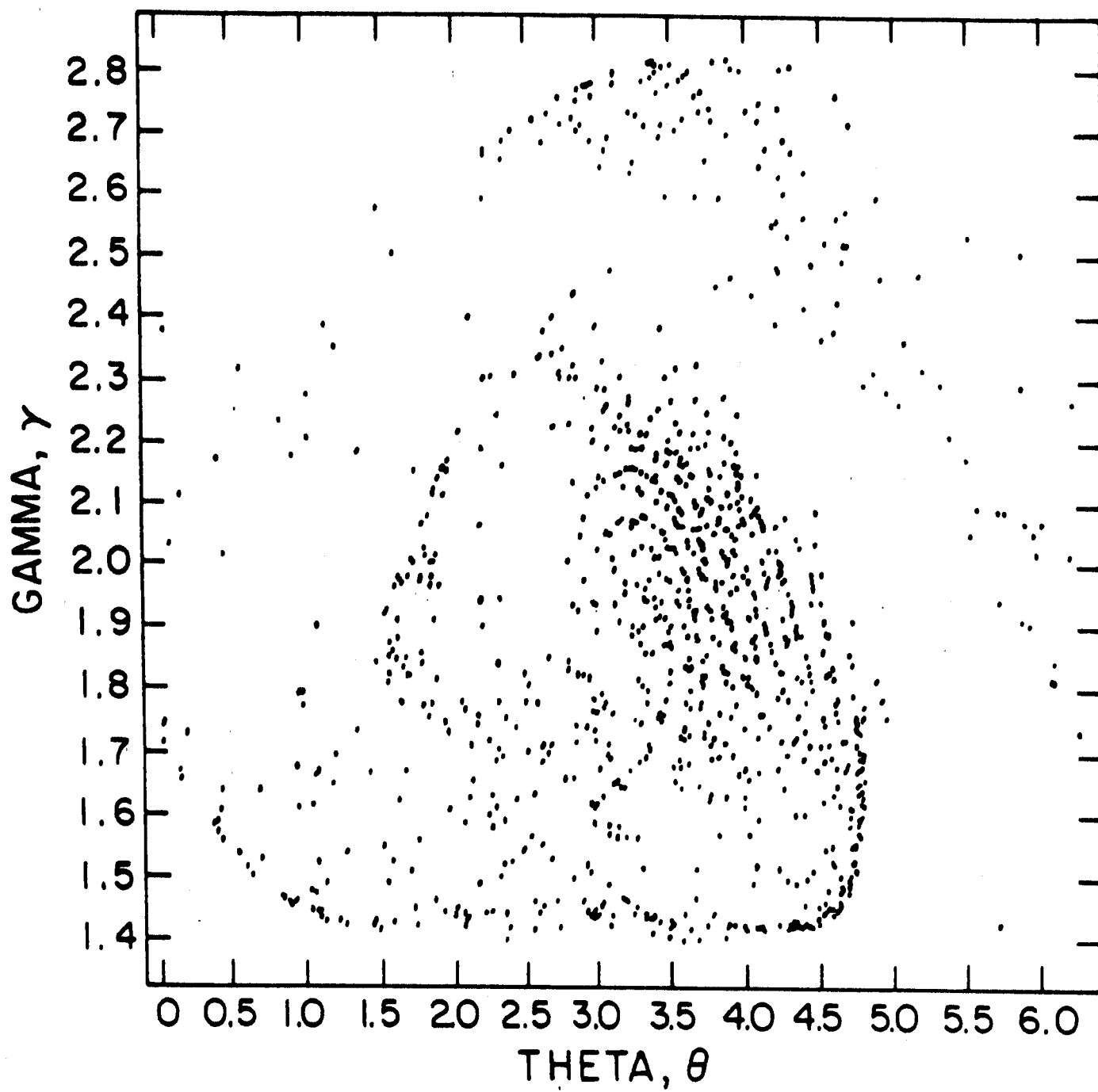


Fig 7.